The Meteoritical Society

Meteoritics & Planetary Science 1–13 (2023)
doi: 10.1111/maps.14106

Olivine microstructure and thermometry in olivine-phyric shergottites Sayh al Uhaymir 005 and Dar al Gani 476

Eleanor S. JENNINGS [1,2]* and Peter COULL[2,3]

[1]Birkbeck, University of London, London, UK
[2]The Centre for Planetary Sciences at UCL/Birkbeck, London, UK
[3]University College London, London, UK
***Correspondence**
Eleanor S. Jennings, Birkbeck, University of London, Malet Street, London WC1E 7HX, UK.
Email: e.jennings@bbk.ac.uk

(Received 09 August 2022; revision accepted 08 November 2023)

Abstract–Olivine-phyric shergottites are relatively young Martian meteorites that resemble primitive mantle-derived melts, so offer insight into the causes of recent magmatism on Mars. The Al-in-olivine geothermometer offers the potential to examine (near-)liquidus melt temperatures. However, the ubiquitous shock features in most Martian meteorites, caused by high-energy impacts, can change the structure and composition of olivine crystals, making the applicability of mineral geothermometry methods uncertain. This study examines microstructure and mineral chemistry in two shocked primitive, depleted olivine-phyric shergottites, Sayh al Uhaymir (SaU) 005 and Dar al Gani (DaG) 476. DaG 476 is unsuitable for Al-in-olivine thermometry because of the presence of difficult-to-observe but pervasive networks of undulating veins in olivine down to sub-micron sizes, caused by melting and providing pathways for cation diffusion. In contrast, SaU 005 can be used for Al-in-olivine thermometry despite the presence of conjugate shear and fracture sets and micron-scale cpx-spinel exsolution. The average crystallization temperature of $Fo_{>70}$ olivine in SaU 005, 1380°C, is near-identical to the average temperature of new and published $Fo_{>70}$ data from all olivine-phyric shergottites. When corrected for equilibrium with mantle olivine (Fo_{80}) this corresponds to a mantle temperature of approximately 1500°C, 130°C hotter than ambient Martian mantle when shergottites formed. Shergottites were generated by melting within a moderately hot mantle plume or thermal anomaly, in support of other evidence that the Martian mantle is actively convecting. However, it does not support the extremely high potential temperatures estimated for the shergottite source by a whole-rock petrological method.

INTRODUCTION

Evidence for recent volcanism on Mars (e.g., Horvath et al., 2021) as well as the young ages of many shergottites (e.g., Lapen et al., 2017) show that Mars' interior is still convecting and, in places, hot enough to melt. Olivine-phyric shergottites are primitive rocks that are thought to be the products of melting within the Martian mantle. As such, they contain useful information to constrain the thermal structure and history of Mars. Several relevant mineral thermometers have been developed for terrestrial igneous systems (e.g., Coogan et al., 2014; Köhler & Brey, 1990; Putirka, 2008); because compositions of Martian meteorites are fairly similar to mafic magmas on Earth (e.g., Tait & Day, 2018; Treiman & Filiberto, 2015), those geothermometers should be applicable to Martian materials. By using thermometry techniques to determine the near-liquidus crystallization temperatures of these shergottites, it should be possible to understand the temperature of their mantle source. This would aid our understanding of how mantle plumes function on Mars and how the planet has thermally evolved.

The Al-in-olivine thermometer was calibrated by Wan et al. (2008) and Coogan et al. (2014). The solubility of Al in olivine is temperature dependent and the thermometer is formulated in terms of the exchange of Al between olivine and spinel. It is therefore applicable to most olivines from primitive magmas that co-crystallized with, and were thus in equilibrium with, spinel, for example as olivine containing spinel inclusions (Coogan et al., 2014; Jennings et al., 2019; Prissel et al., 2017a). Its use requires no knowledge of the melt composition. Unlike Fe-Mg exchange thermometers, the relatively low diffusivity of Al in the olivine structure should make it robust to re-equilibration during subsolidus cooling or brief high-temperature impact events (Chakraborty, 1997; Spandler and O'Neill, 2010); indeed, the lower temperatures from Fe-Mg exchange thermometry compared to Al-in-olivine thermometry of olivine-phyric shergottites has been attributed to subsolidus cooling (Ramsey et al., 2021). On Earth it has proved useful in demonstrating that many continental flood basalt provinces owe their existence to mantle plumes (Coogan et al., 2014; Heinonen et al., 2015; Jennings et al., 2019; Xu & Liu, 2016), and it has recently been applied to some extraterrestrial materials: a pallasite (Prissel et al., 2017a) and a range of olivine-pyric shergottites (Prissel et al., 2017b; Ramsey et al., 2021).

Aluminum-in-olivine thermometry looks promising for Martian materials, and its applicability has been argued for on the basis of similarity in igneous composition and yielding similar crystallization temperatures to those expected from experimental studies (Prissel et al., 2017a, 2017b; Ramsey et al., 2021). However, these studies do not consider the robustness of the olivine trace element compositions through a process ubiquitous in meteoritic material: shock. All differentiated meteorites must have experienced significant impact-induced shock associated with their release, which could conceivably redistribute trace elements. Martian meteorites, including the olivine-phyric shergottites, display well-documented alterations caused by shock, such as: melt veins; loss of crystallinity in plagioclase; development of twinning, mosaicism, deformation and fractures in crystals; and the presence of high-pressure phases (e.g., Sharp & de Carli, 2006; Walton et al., 2014). Olivine phenocrysts specifically can develop a brown color from metal exsolution, planar fractures, dislocations, mosaicism, and other microstructural crystallographic changes such as the development of planar features that may be associated with phase transitions during shock metamorphism (Greshake et al., 2004; Greshake & Stöffler, 1999; Takenouchi et al., 2018; Van de Moortèle, Reynard, McMillan, et al., 2007; Van de Moortèle, Reynard, Rochette, et al., 2007). Different olivine-phyric shergottites display different shock features, thought to be caused by varying peak pressures, temperatures, and subsequent cooling paths. In addition, some meteorites experienced a protracted exposure history on Earth's surface, resulting in low-temperature weathering-related alteration (e.g., Zipfel et al., 2000).

The wide array of shock features that affect olivine crystals have the potential to cause localized redistribution of trace elements, and fractures and veins expose the grain interior to the diffusive addition or loss of elements from external sources. This does not necessarily mean that thermometry based on trace element concentration is not possible. It does, however, warrant a careful consideration of the effect of shock and alteration processes on trace element distribution in order to demonstrate applicability of trace element thermometers.

In this study, two olivine-phyric meteorites are examined, DaG 476 and SaU 005. These heavily shocked meteorites are petrologically similar but display different shock effects and post-igneous histories. Their suitability for thermometry is examined in the context of microstructure and alteration; Al-in-olivine thermometry is then carried out on SaU 005, as DaG 476 was found unsuitable. New thermometry data are combined with published data to infer the thermal conditions of their mantle sources.

MATERIALS AND METHODS

Samples

Two primitive depleted olivine-phyric basaltic shergottite samples, DaG 476 (BM.2000,M7) and SaU 005 (BM.2000,M40), were selected for this study. These samples are petrologically similar but have somewhat different impact and terrestrial exposure histories. They are primitive magmatic rocks, with abundant and moderately high forsterite (up to Fo_{73}) olivine phenocrysts with spinel inclusions. Both rocks are over-abundant in olivine according to their whole-rock Mg/Fe (Papike et al., 2009), which is not a problem for mineral–mineral thermometry. Their olivine forsterite contents are moderately high in terms of the Martian meteorite record, which reaches a maximum of Fo_{85} (Gross et al., 2011). This is low compared to primitive olivine on Earth because the Martian mantle has a high Fe-Mg relative to Earth. These samples are therefore well-placed to investigate Martian mantle processes. However, they are both affected by both shock metamorphism from their excavation, and DaG 476 is affected more extensively by weathering from its time on Earth's surface, which complicates the link of both meteorites to the Martian mantle.

Dar al Gani (DaG) 476

DaG 476 (paired with DaG 489) consists of ~15 vol% of mm-sized euhedral $Fo_{60\text{-}77}$ (Papike et al., 2009)

olivine macrocrysts (phenocrysts) with Cr-spinel inclusions in a groundmass of pyroxenes, feldspathic glass and minor oxides, sulfides, and phosphates (Zipfel et al., 2000).

Shock features such as melt veining, maskelynite, and pyroxene twinning are ubiquitous signs of impact damage. Specifically in the olivine, fracture, mosaicism, dislocations, micro-scale melt veining, and browning have been described (Greshake & Stöffler, 1999, 2000). Shock features suggest peak pressure conditions of 40–45 GPa, though the lack of high-pressure phases implies a rapid cooling and decompression rate (Greshake & Stöffler, 2000). Of particular note is the description of planar and irregular fractures and melt-filled veins that are 0.2–0.4 μm wide by Greshake and Stöffler (2000); these features were found to be frequent in olivine that was thermally metamorphosed by nearby melt veins, identified in ATEM images. Greshake and Stöffler (2000) attribute these and other features to post-shock heating following a shock event. More recently, Miyahara et al. (2011) did identify high-pressure phases in DaG 735, suggested to be paired with DaG 476: nm-scale perovskite and magnesiowüstite was found in olivine adjacent to a melt vein. This was interpreted as the product of olivine dissociation at the somewhat lower-pressure conditions of 25 GPa and >700°C.

Secondary calcite is common along grain boundaries and fractures and results from the terrestrial weathering of this meteorite during its extensive residence in the Sahara desert (Zipfel et al., 2000). DaG 476 is a depleted shergottite, although LREE concentrations have been slightly elevated by weathering (Barrat et al., 2001; Mikouchi et al., 2001; Wadhwa et al., 2001; Zipfel et al., 2000).

Terrestrial contamination has prevented the Rb-Sr dating of DaG 476, though Borg et al. (2003) report a Sm-Nd crystallization age of 474 ± 11 Ma. It has a cosmic ray exposure age of 1.17 ± 0.09 Ma (Zipfel et al., 2000) and a terrestrial exposure age of 85 ± 50 ka (Nishiizumi et al., 1999).

Sayh Al Uhaymir (SaU) 005

SaU 005 is compositionally and petrographically similar to DaG 476. It is porphyritic, containing 25% large $Fo_{64\text{-}71}$ olivine phenocrysts, with a groundmass of pyroxene, maskelynite, phosphates, and opaques (Goodrich, 2003; Zipfel, 2000).

Like DaG 476, SaU 005 is strongly shocked. It includes impact melt veins and pockets, maskelynite, pyroxene twinning and fracturing, and olivine mosaicism and planar deformation features (Boctor et al., 2001; Goodrich, 2003; Papike et al., 2009); the different features are interpreted as resulting from a wide range of shock pressures from shock pressures of 28 to >60 GPa by Boctor et al. (2001). No high-pressure phases have been identified. In published studies, the melt veining and recrystallization in SaU 005 is less prominent than DaG 47. Unlike DaG 476, SaU 005 is fresh and shows little evidence of weathering, with only trace carbonate in fractures (Zipfel, 2000). Along with DaG 476, SaU 005 is one of the most depleted shergottites in terms of trace elements and εNd (Dreibus et al., 2000).

SaU 005 has a Sm-Nd crystallization age of 445 ± 18 Ma (Shih et al., 2007); cosmic ray exposure age of 1.5 ± 0.3 Ma; and an assumed short terrestrial age (Pätsch et al., 2000) and is suggested to have a paired ejection with DaG 476 (Nyquist et al., 2001).

Analytical Methods

A JEOL JXA-8100 electron probe micro-analyzer (EPMA) instrument at Birkbeck, University of London, was used to acquire images, elemental maps, and quantitative data of carbon-coated thin sections. A 15 keV accelerating voltage was used. BSE images were collected with a focused 10 nA beam.

Quantitative EDS, using an Oxford Instruments detector, was used for initial compositional characterization and for producing elemental distribution maps using a focused 20 or 25 nA beam.

WDS was used for point analyses of olivine and spinel pairs, with spinel inclusions hosted within olivine phenocrysts, and for trace element distribution mapping. Point analyses were performed on spinel inclusions and their neighboring olivine host, with olivine measurements made on three sides of the spinel where possible. A distance of at least 10 μm was left from the edge of the spinel when measuring olivine in order to avoid additional Al signal from secondary fluorescence (Jennings et al., 2019).

Point WDS analyses were made at 50 nA with a focused beam. Olivine analyses were calibrated on natural and synthetic standards, with peak counting times (s) given after the standard material: Mg, Si, Fe (olivine, 20); Al (corundum, 300); P (apatite, 60); Ca (wollastonite or diopside, 60); Cr (Cr metal, 40); Mn (Mn metal, 20); Ni (Ni metal, 40). Backgrounds were measured for half the peak counting time. Spinel analyses used the same calibration with additional Ti (rutile or ilmenite) with all elements measured for 20 s. A φρz correction was applied. Calibrations were checked with a BCR-2G secondary standard.

For semi-quantitative elemental maps in olivine, a 25 nA focused beam was used and the stage was rastered. Aluminum was either measured in tandem by two spectrometers with TAPH crystals, or was measured on one spectrometer with Si on the other. Potassium was measured on a third spectrometer with a PETH crystal. A forsterite composition was assumed for the matrix

correction in the quantification, calculated by the in-built JEOL software.

All point analyses of olivine and spinel had acceptable EPMA totals (olivine: 99.7–101.7 in SaU 005; 98.0–102.2 wt% in DaG 476); spinel: 96.8–100.8 wt% following correction for Fe_2O_3 following the method of Droop, 1987) and no olivine or spinel data were initially filtered from the data set beyond a few misplaced points. The detection limit for Al_2O_3 in olivine was 0.010 wt%. All other detection limits are provided in Table S2.

RESULTS

Microstructure and Compositional Maps

The petrography of the samples of DaG 476 and SaU 005 are consistent with published descriptions (Goodrich, 2003; Papike et al., 2009; Zipfel, 2000; Zipfel et al., 2000), with large (0.5–2 mm) olivine phenocrysts in a fine-grained matrix consisting predominantly of plagioclase (maskelynite in SaU 005) and pyroxenes, with minor oxides. There are a small number of large melt veins and pockets running across both samples (Figure S1).

Olivine in DaG 476 is stained orange-brown and contains a network of irregular, prominent dark brown to opaque melt veins at different scales, in addition to spinel inclusions and melt inclusions (Figure S1a). WDS mapping was performed on small areas in the cores of olivine phenocrysts, to understand the nature of this veining at the small spatial scales relevant to WDS point analyses (Figure 1). The irregular veining is found to be pervasive throughout the phenocrysts, and present at all length scales down to <1 μm, even where it is not easily visible in BSE images. These veins are similar to those described by Greshake and Stöffler (2000). This veining is associated with a compositional change: veins are rich in Al, Si, and K relative to olivine. Up to ~2.8 wt% K_2O and ~1.3 wt% Al_2O_3 are identified in thicker parts of the veins; lower concentrations in thinner parts of the veins are likely because the veins are narrower than the electron beam and the analyses more contaminated by olivine.

The elemental heterogeneity caused by the dense, pervasive veining extends to length scales smaller than those that can be analyzed by standard EPMA. Because of this, it is impossible to avoid, and because additional Al may have been added during weathering, it is not possible to perform Al-in-olivine thermometry on this sample of DaG 476. It should be noted that our thin section is small with few but large olivines: it is unclear if all olivines across all DaG 476 samples are equally affected.

Olivines in SaU 005 contain sub-parallel sets of conjugate fractures and deformation features, in addition to spinel inclusions (infrequently in olivine cores, frequently off-center and in rims) and primary melt inclusions (Figure 2). In Figure 2b, an E-W set of internally featureless parallel bands is seen. Surrounding olivine contains a set of short conjugate fractures that often terminate at the bands. The fine-scale pervasive veining present in DaG 476 is absent in phenocrysts in SaU 005. EDS mapping shows that the bands have a similar composition as the surrounding olivine, and there is no evidence of these bands being vectors for chemical diffusion (Figure 3). The same is true of the short conjugate fractures (Figure 3). In addition, the bands are clear enough to see and widely enough spaced that they can be avoided during WDS point analysis.

Olivine phenocrysts in SaU 005 also contain pervasive fine-grained (1–3 μm) particles that are bright in BSE images; these are absent in DaG 476. The bright spots are fairly uniformly sized and distributed, though are not found in the deformed bands. These were investigated by high-magnification EDS mapping (Figure 3). The spots contain high concentrations of Cr, Ca and Al relative to the host olivine, low Mg, and no obvious elevation in K or Fe. The particles appear to be fine two-phase intergrowths. The phases are too small to measure individually but the compositional information suggests that they may be Cr-spinel-clinopyroxene intergrowths. There are areas of olivine that have few of these particles, spaced far enough apart (10s of micrometers) that point analyses can be made that avoid them, and accidental inclusion of these particles in an analysis should be obvious from Ca and Cr concentrations. Olivine phenocrysts in SaU 005 may therefore be used for Al-in-olivine thermometry. In this study, no data from olivine phenocrysts in SaU 005 were filtered out.

Olivine and Spinel Composition

Olivine measured with the intention of thermometry (i.e., near spinel) in DaG 476 is $Fo_{60.1}$ to $Fo_{72.1}$ and spinel inclusions have Cr# ($=X_{Cr}/[X_{Cr} + X_{Al}]$, mol fraction) 0.690–0.875. Olivine similarly measured in SaU 005 is $Fo_{63.3}$ to $Fo_{73.3}$ ($Fo = 100X_{Mg}/[X_{Mg} + X_{Fe}]$) and spinel inclusions have Cr# 0.697 to 0.855, consistent with the detailed characterization of spinels in SaU 005 by Goodrich (2003). The full data set is provided in Table S1 alongside uncertainties in Al_2O_3 in olivine, with all other uncertainties reported in Table S2 and the thermometry results for SaU 005 are shown in Table 1.

Point analyses were made in olivine phenocrysts in both samples with the intention of performing Al-in-olivine thermometry. However, the apparent unsuitability of meteorite DaG 476 for this technique is confirmed by the data (Figure 4). Despite careful efforts to avoid veined olivine and to analyze only regions that appeared "clean" in BSE images, erratic and high-Al and Cr concentrations

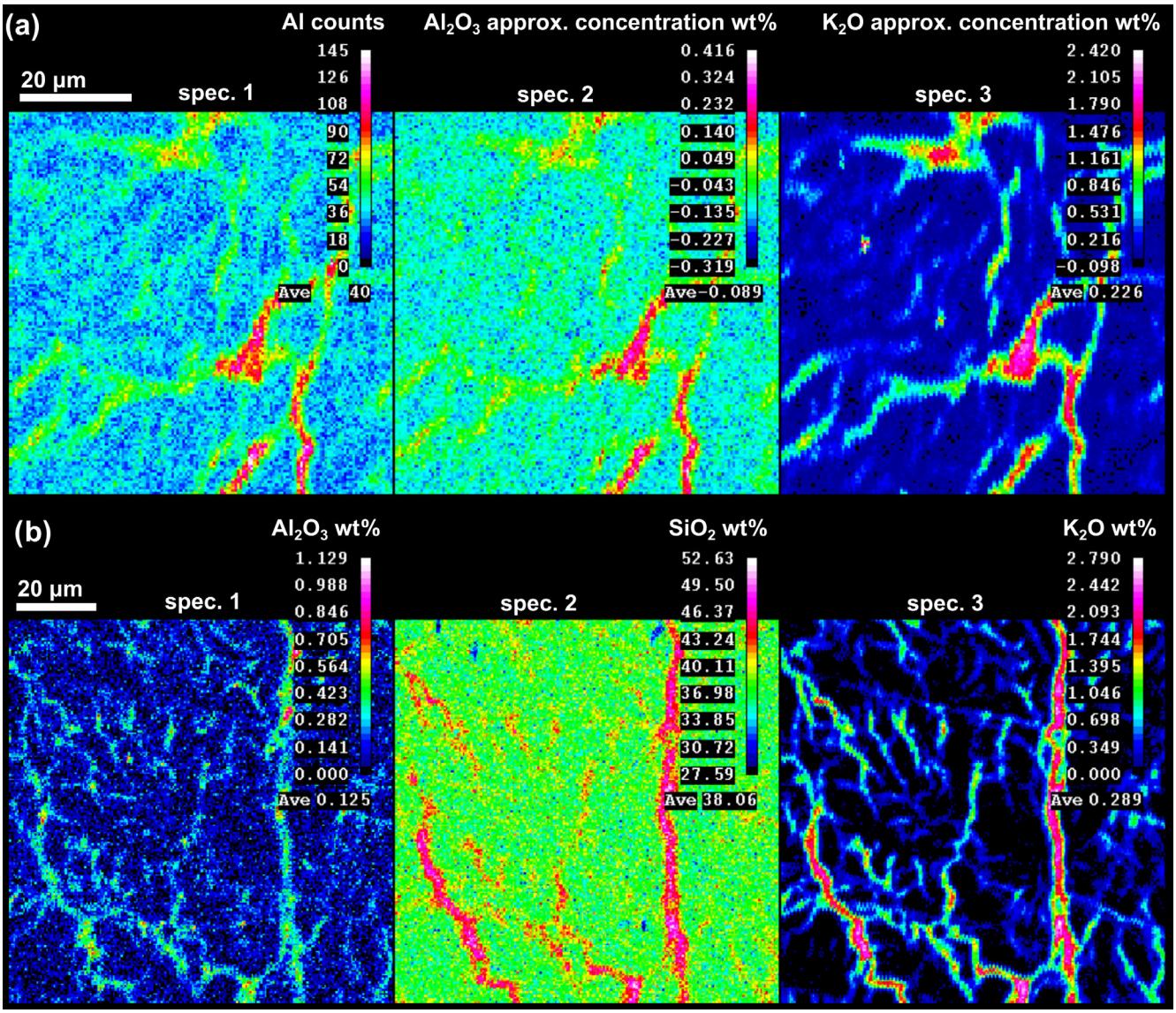

FIGURE 1. DaG 476: WDS maps of two different locations near the center of a large olivine phenocryst. Bright colors are high count intensities; 0.5 × 0.5 μm pixel size (step length). (a) Al (left, center) and K (right) were analyzed; on spectrometer 1, counts are shown, on 2 and 3, approximate wt% concentrations were calculated using the standard k-ratio. Note that these concentrations are only approximate because backgrounds, full standardization, and matrix correction were not used for this map. Dwell time 35 ms, eight accumulations. (b) Al (left), Si (center) and K (right); wt% oxide (assuming a forsterite MgO concentration for matrix corrections; see Methods). Dwell time 30 ms, six accumulations. In all cases, concentrations are imprecise because of short count times per pixel.

(0.006–0.697 wt% Al_2O_3 and 0.05–1.24 wt% Cr_2O_3) are present in many (but not all) analytical points in olivine phenocrysts from DaG 476 that must result from the micro- to nano-scale veining discussed in Samples section. Filtering these data by assuming an arbitrary maximum Al_2O_3 concentration could skew the temperature distribution in the remaining data, and other trace element elevations are not straightforwardly correlated with Al_2O_3. No further efforts are therefore taken in using DaG 476 for thermometry.

In contrast, the range of olivine compositions observed in SaU 005 is much more limited, with lower Al_2O_3 (0.011–0.096 wt%) and Cr_2O_3 concentrations (0.04–0.31 wt%) that are more consistent with olivine analyses from primitive samples from Earth (Coogan et al., 2014; Jennings et al., 2019). Ni ranges from 246 to 556 ppm. P_2O_5 is low (<0.1 wt%) in all olivines and uncorrelated with Al, so a coupled P–Al substitution mechanism is not significant and required no correction (cf. Coogan et al., 2014). Minor element concentrations

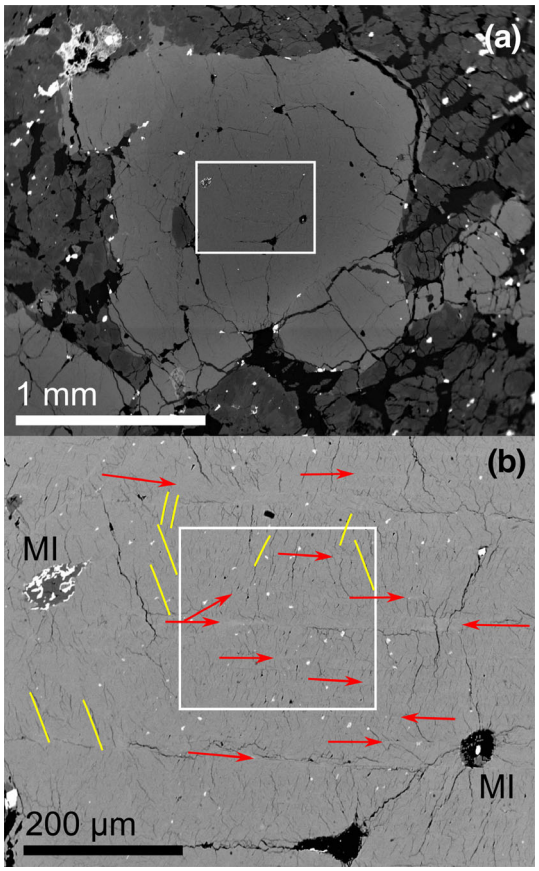

FIGURE 2. BSE image of (a) a 2 mm phenocryst in SaU 005 and (b) a higher-magnification image of the core region. The white box in (a) shows the location of image (b). MI, melt inclusion. In (b), the melt inclusion on the left is pristine but crystallized, whereas the one on the right has been partially lost from the slide, which is more usual for secondary phases in breached inclusions. A set of short conjugate fractures that terminate within the crystal are highlighted by yellow lines. They terminate against a set of parallel deformation features, some examples of which are shown with red arrows. White box shows location of image in Figure 3.

are weakly correlated to uncorrelated; relationships between minor element concentrations are shown in Figure S2.

For most elements measured in spinel, the Al-in-olivine thermometer is also straightforwardly applicable. $Fe^{3+}{}_{spinel}$ could introduce uncertainty by replacing Al on the spinel M1 site, but all Fe^{3+}/Fe_T in spinels in this study are at the low end of the range in the calibration set. The Al-in-olivine thermometer is only calibrated with low-Ti spinels, so the SaU 005 data set of ol-spinel pairs was filtered to remove the two spinels with ≥0.03 Ti per formula unit (p.f.u.). The Al-in-olivine thermometer is also only calibrated with spinels in the range Cr# = 0–0.69, despite the frequent occurrence of spinels with Cr# >0.69 in primitive rocks on Earth and on Mars. The spinel Cr# range here is above that, reflecting a relatively low activity of Al. We make the assumption that the thermometer is still applicable because (i) published thermometry results comparable with experimental ones (Prissel et al., 2017b; Ramsey et al., 2021) and (ii) the relationship between $Cr\#_{spinel}$ and $\ln(k_d)$ shown by Wan et al. (2008) is unambiguously linear and would presumably extrapolate linearly (except perhaps at the lowest experimental temperature of 1250°C). The relationship between Ti content and Cr# of the filtered spinels is shown in Figure S3.

Al-in-Olivine Thermometry

The Al-in-olivine temperature of spinel-olivine pairs was determined using the equation of Coogan et al. (2014):

$$T(\mathrm{K}) = \frac{10,000}{0.575(0.162) + 0.884(0.043)\mathrm{Cr\#} - 0.897(0.025)\ln(k_d)}$$

where $k_d = Al_2O_3{}^{olivine}/Al_2O_3{}^{spinel}$ in wt% and the values in parentheses are the published SE of the parameter. Results for SaU 005 are reported in Table 1.

Olivine-spinel pairs were not filtered by Fe-Mg equilibrium because the high contrast in diffusivity of Mg and Fe versus Al in olivine (Chakraborty, 1997; Spandler and O'Neill, 2010) means that the two systems are decoupled, that is, equilibrium in one system does not imply equilibrium in the other. This explains the difference in Fe-Mg versus Al temperatures identified in shergottites by Ramsey et al. (2021). It is assumed that olivine and spinel were both in equilibrium with the melt they co-crystallized from, as suggested by their morphologies in SaU 005, and that Al contents are frozen into those phases when spinels are trapped as inclusions. While impact-driven elevated temperatures and their durations are not well known, in SaU 005 at least they were insufficient to melt olivine. Given that the diffusion of Al is negligible at the timescale and temperatures of experimental diffusion studies, and at least two orders of magnitude slower than the major cations (Spandler and O'Neill, 2010), it is unlikely that Al diffused significantly as a result of impact heating. However, Table 1 does indicate heterogeneity in Al concentrations and temperatures in olivine around some of the spinel inclusions, implying that one or more of these assumptions does not always hold true on a local scale. Outlier individual temperature data points in this study and in those of Ramsey et al. (2021) should therefore still be interpreted with caution.

The average Al-in-olivine temperature of all SaU 005 analyses is 1300 ± 130°C (1 SD). The individual Al-in-olivine temperatures have a large range (Figure 5), even when considering the propagated analytical error, which for all temperatures except one is larger than the inherent thermometer uncertainty of ±11°C (Coogan et al., 2014;

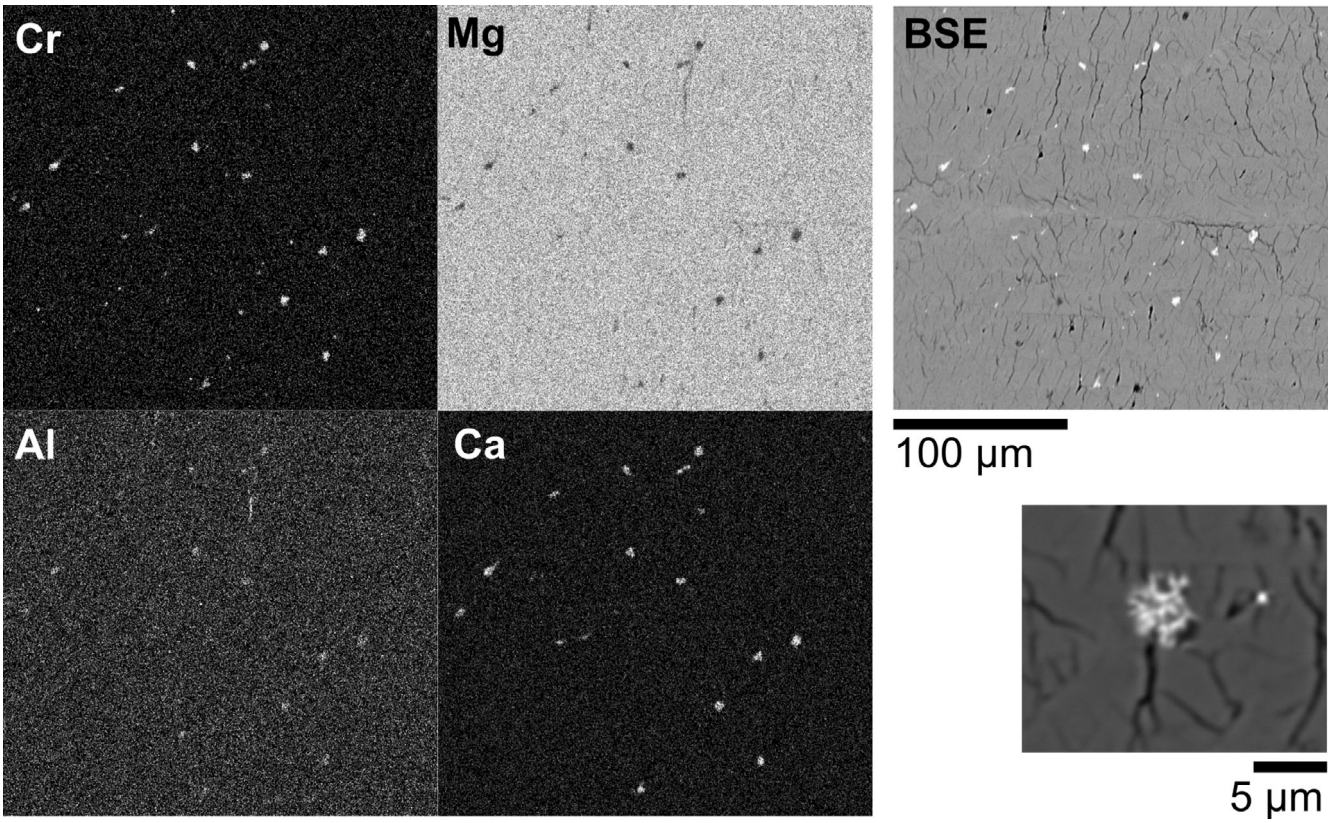

FIGURE 3. SaU 005: EDS map of a small area in the center of a large olivine phenocryst. Bright regions are higher count rates. Right top: EDS images of the same region. Right bottom: high-magnification BSE image of one of the bright spots, which appears to show a two-phase mineral intergrowth, one bright and the other darker than the surrounding olivine. Dark irregular lines on BSE images are small fractures interpreted as a shock metamorphism feature.

Jennings et al., 2019). There is only a weak trend of decreasing temperature with decreasing Fo, as would be expected from crystallization (vector shown in Figure 5). Because the range of Fo contents of the different olivine measurements is small, the small decrease in T with Fo that would be expected may be obscured by analytical uncertainty and by the redistribution of Fe-Mg by subsequent cooling and heating, for example, during impacts. The mean Al-in-olivine temperature for the cluster of six Fo $>$ 70 olivine analyses is 1380 $\pm$ 150°C. Because their Fo contents are close to the sample maximum ($Fo_{73.3}$), these temperatures are close to the liquidus of SaU 005.

DISCUSSION

Origin of Microstructural Features

The fine veins in olivine in DaG 476 do not follow fractures, are extremely small, are pervasive, and have undulating, branching forms. It is unlikely that an external melt could penetrate in this way; thus, we suggest that the veins are probably originally magmatic in nature, that is, they were shock melts that originated from partial melting internally within the olivine, rather than penetrating the olivine from external sources. These may be the sub-micron veins described by Greshake and Stöffler (2000), but they appear in all olivine regardless of proximity to major melt-filled fractures. The chemistry of the veins must have been altered since their igneous formation. The concentration of K is significantly higher than Al in these veins, whereas the concentration of K in pristine olivine is negligible and lower than that of Al because the large radius of K^+ makes it highly incompatible. K^+ is, however, fluid-mobile. This points to an interpretation where weathering and the low-temperature, water-mediated exchange of cations has added additional water-soluble elements to these olivines, where glassy veins provided diffusive pathways through the phenocrysts. This could be feasible given the long residence time of DaG 476 in the Sahara desert (Zipfel et al., 2000). Weathering and shock vein formation are thought to cause yellow and brown coloration of olivine, respectively (Takenouchi et al., 2018), so this interpretation is consistent with the patchy yellow-brown tinge of some of olivine phenocrysts of DaG 476 (Figure S1).

TABLE 1. Selected aspects of mineral chemistry and temperature calculation for olivine-spinel pairs in SaU 005. Calculated temperature uncertainties are based on uncertainty in the Al measurements. Complete analytical data are provided in Table S1.

Spinel				Olivine					
#	Al_2O_3 wt%	Ti p.f.u.	Cr#	#	Al_2O_3 wt%	Fo	T	$+1\sigma$	-1σ
1	9.3	0.024	0.80	1	0.020	65.4	1202	30	34
				2	0.048	66.6	1393	17	17
				3	0.060	64.7	1447	14	15
2	11.6	0.027	0.75	1	0.038	67.7	1298	19	20
				2	0.027	67.7	1221	24	26
				3	0.012	67.4	1081	40	50
3	9.9	0.016	0.80	1	0.020	72.2	1192	29	33
				2	0.033	71.8	1291	21	23
				3	0.096	71.6	1566	11	11
6	9.4	0.019	0.80	1	0.082	73.0	1533	12	12
				2	0.035	72.5	1313	21	22
				3	0.049	73.3	1393	16	17
7	9.6	0.028	0.80	1	0.053	66.5	1409	16	16
				2	0.015	66.0	1143	36	43
				3	0.026	67.6	1248	25	28
8	6.9	0.012	0.85	1	0.022	69.2	1270	30	34
				2	0.062	68.8	1524	15	16
				3	0.032	66.6	1351	24	26
9	9.2	0.017	0.80	1	0.027	67.3	1263	25	27
				2	0.022	68.0	1219	29	32
				3	0.025	66.3	1250	26	28
10	7.1	0.016	0.85	1	0.015	66.8	1188	39	45
				2	0.024	66.8	1283	28	31
				3	0.014	67.0	1174	41	48
11	9.3	0.021	0.80	1	0.011	65.9	1084	47	60
				2	0.057	66.5	1435	15	16
				3	0.026	66.4	1256	25	27
12	10.6	0.022	0.77	1	0.021	66.4	1191	28	32
				2	0.041	67.0	1328	18	19
				3	0.056	68.7	1407	15	15

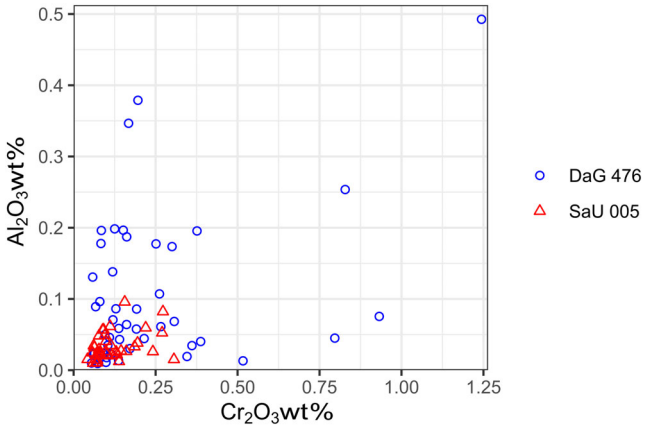

FIGURE 4. Al_2O_3 and Cr_2O_3 concentrations in wt% measured in olivine phenocrysts in DaG 476 and SaU 005. Vertical 2σ error bars approximately the same size as the symbols; horizontal are smaller than the symbols.

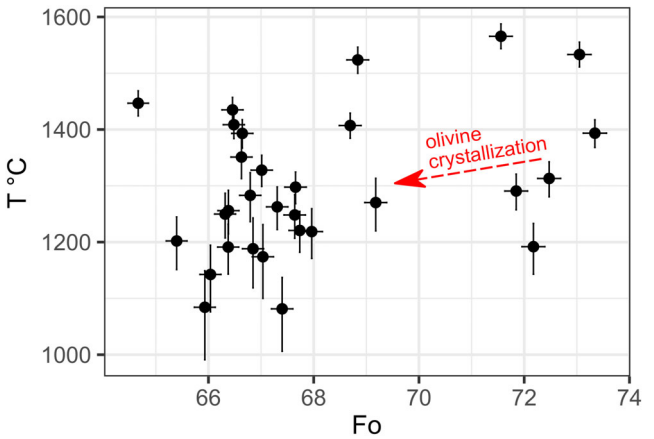

FIGURE 5. Al-in-olivine temperature as a function of olivine Fo content in sample SaU 005. Error bars are 2σ uncertainty. Olivine crystallization vector (red arrow) of $dT/dFo = 16$ was calculated by modeling SaU 005 fractionation in Petrolog3 at QFM-2 (Danyushevsky & Plechov, 2011).

The parallel featureless bands in SaU 005 (Figure 2) appear to be an example of optically dark bands (ODB) that have been described from other Martian meteorites with particularly dark brown olivines (Van de Moortèle, Reynard, McMillan, et al., 2007; Van de Moortèle, Reynard, Rochette, et al., 2007), though olivine in SaU 005 is not particularly brown (Figure S1) and the ODBs are rather thin and form a small minority of the olivine (Figure 2). As in the study of Van de Moortèle, Reynard, Rochette, et al. (2007), we also find that these bands do not have a resolvable different composition to surrounding olivine by EDS mapping. Optically-dark bands were found by Van de Moortèle, Reynard, Rochette, et al. (2007) to be characterized by high crystallinity; they are crystallographically continuous with the surrounding fractured olivine so are part of the original crystal rather than being recrystallized melt veins. Such parallel bands or lamellae have been interpreted as resulting from a transient phase change to a high-pressure olivine polymorph during shock, without melting (Takenouchi et al., 2018; Van de Moortèle, Reynard, McMillan, et al., 2007). We interpret these as a high-pressure shock feature that post-date the formation of the fine conjugate fractures that terminate against them.

The fine-grained clinopyroxene-Cr-spinel intergrowths are pervasive throughout the phenocrysts, though distanced apart enough that they are easily avoided when analyzing olivine. Their origin is not immediately apparent. Khisina et al. (2013) identified chromite–diopside symplectite inclusions in olivine from lunar

regolith. To explain their formation, the authors proposed a diffusion-controlled mechanism whereby Cr and Ca, originally minor elements from within the olivine structure, diffuse towards, and nucleate at, olivine defects, combining with Si, Mg and Fe to precipitate symplectites of chromite and diopside, during decompression. Furthermore, this symplectite formation is suggested to involve the oxidation of divalent Cr, driven by the dehydrogenation of OH-bearing point defects in the olivine, at high temperatures of >800°C (Khisina et al., 2013; Khisina & Lorenz, 2015). Disturbances to the Cr_2O_3 of the host olivine were limited to a few tens of micrometers from the edges of the symplectites, with less disturbance to less diffusive elements.

Augite–magnetite symplectites have also been reported in olivine from the Nakhla Martian meteorite, driven by a similar mechanism involving the oxidation of divalent iron rather than chromium (Mikouchi et al., 2000; Mikouchi & Miyamoto, 1998). The oxygen fugacity of Martian primitive magmas is higher than those of the Moon: Khisina and Lorenz (2015) note that the spinel phase produced by dehydrogenation-driven oxidation would depend on the oxygen fugacity of a particular sample, that is, whether divalent Cr or Fe is present to be oxidized. Therefore, a viable explanation for the presence of the <10 μm chromite–clinopyroxene micro-inclusions in SaU 005 is the exsolution of components originating from within the olivine, perhaps mediated by dehydrogenation at low fO_2. The timing of their precipitation is unknown.

Evidence for the preservation of the original olivine structure in SaU 005 is further provided by the presence of primary melt inclusions that contain igneous minerals (Figure 2b). This suggests that, despite the shock event, the olivine structure was largely unaffected beyond the creation of fractures and sparse parallel bands. The chemical composition of the olivine should also, therefore, be preserved.

Effect of Microstructure on Olivine Minor Element Composition

Igneous meteorites have a complicated history compared to terrestrial igneous rocks, because they have experienced shock metamorphism during the impact that released them from a planetary surface, perhaps experiencing prior additional shock events; some also experienced a protracted exposure history on Earth's surface. These processes can disturb the major and minor element composition of olivine phenocrysts.

The veining in DaG 476 is extremely fine in places, and difficult to see in BSE images if not specifically looked for. It is pervasive, and cannot be avoided. It is characterized by notably elevated K concentrations; K is not typically included in WDS analyses of olivine, so disturbances to the olivine compositions might be missed, making data difficult to interpret. In this study, Al concentrations in point analyses of DaG 476 olivine were often erratically elevated and not well-correlated with other measured elements. Their origin was difficult to diagnose but is presumably due to unintentional measurement of a sub-micron vein. On the other hand, SaU 005 was free of pervasive melt veining, and the shock features identified in its olivine phenocrysts were either avoidable (e.g., the spinel-clinopyroxene intergrowths) or else had no bearing on the analysis, as evidenced by typical minor and trace element (Ca, Cr, Ni, P, Mn) concentrations. We recommend the inclusion of a fluid-mobile minor element such as K in routine measurements of silicate minerals in meteorite samples to assist in the identification of similar cryptic alteration, and that meteorites are assessed on a case-by-case basis for suitability for the technique. Unlike DaG 476, SaU 005 has maintained, on the whole, crystallographic and compositional integrity.

Ramsey et al. (2021) compare Al-in-olivine results for several olivine-phyric shergottites with experimental and other studies on those samples to confirm the applicability of the thermometer. The crystallization temperatures, representing near-liquidus temperatures, are generally in good agreement with experimental studies, indicating that those olivines maintained their integrity through shock and subsequent processes. However, there is a notable exception: a subset of olivine analyses contained very high-Al concentrations (1000–3000 ppm); these were excluded from thermometry because the concentrations were considered unreasonably high, with a suggestion that they originate from fluorescence of characteristic Al-kα x-rays from nearby spinel inclusions (Ramsey et al., 2021). However, in addition to the stated reason, Al could be elevated for several other reasons relating to shock history, including elemental redistribution and the opening of diffusional pathways by internal melting, shearing and other shock processes, and not always be elevated by such a noticeable extent. For example, high-Al olivine measurements from NWA 1068 were excluded by Ramsey et al. (2021); this meteorite contains olivine that has undergone transformation to high-pressure phases in the vicinity of shock melt pockets, and have become discolored (Takenouchi et al., 2018). Likewise, Tissint olivines show clear evidence for shock alteration (Walton et al., 2014). While shock features are not necessarily a problem, as they are not for SaU 005, this does warrant consideration.

Crystallization Temperature and Melting of the Mantle Source of Shergottites

Data from this study are combined with that of Ramsey et al. (2021) in Figure 6. Overall, only a weak

correlation is seen between Fo content and temperature (Figure 6). Depleted and enriched shergottite Al-in-olivine temperature measurements have similar ranges and means, so there does not appear to be an important difference between the different sub-groups of olivine-phyric shergottite in terms of crystallization temperature (Ramsey et al., 2021).

The average temperature measurement of all reported shergottite data is 1320°C (standard error, SE = 20°C). This rises to 1380°C (SE = 20°C at a mean Fo of 72.7) if only those olivines with Fo > 70.0 are considered, that is, the 21 most primitive olivine measurements. These data are consistent with a preliminary Al-in-olivine temperature of ~1360°C presented by Prissel et al. (2017b) for primitive shergottite NWA 5789, which potentially represents one of the most primitive and mantle-like measurements given that NWA 5789 contains up to Fo_{84} olivine (although the forsterite content for the thermometry was not stated).

Olivine crystallization temperatures provide a minimum constraint for mantle temperature, because the mantle source cannot have been cooler than the crystallizing melt. However, the Martian mantle source of shergottitic melts is likely to have been much hotter than these temperatures, because high-Fo olivines are still around 10% lower Fo than Fo_{80} mantle olivine (implied by the bulk Mars composition of Yoshizaki & McDonough, 2020), indicating prior olivine fractionation. By taking $\frac{dT}{dFo} = 16$°C/Fo (calculated by modeling SaU 005 fractionation in Petrolog3, Danyushevsky & Plechov, 2011, at QFM-2), the corrected mean temperature in equilibrium with Fo_{80} mantle olivine is approximately 1500°C. The minimum temperature of the mantle source of shergottite melts is therefore around 1500°C. If the mantle is instead Fo_{84}, that is, the highest-Fo olivine found in shergottites, then the corrected temperature would be a less-conservative 1560°C. The actual mantle potential temperature (T_P, the mantle temperature corrected to zero pressure if no melting occurred; McKenzie & Bickle, 1988) would be a little higher because of the cooling effects of adiabatic decompression and the enthalpy of fusion.

The ambient potential temperature for Mars' mantle during the Amazonian is around 1370°C (Baratoux et al., 2011; Filiberto, 2017), which is comparable to Earth's mantle at that time (Herzberg et al., 2007). Olivine-phyric shergottites therefore appear to derive from anomalously warm mantle, with a lower bound on the temperature offset of around ΔT ~130°C. A mantle thermal anomaly is most straightforwardly interpreted as a convective upwelling of unusually hot rock, that is, a mantle plume on Earth (e.g., Herzberg & Gazel, 2009), and we interpret it as such on Mars. This temperature offset is comparable to typical plumes on Earth (e.g., Herzberg & Gazel, 2009).

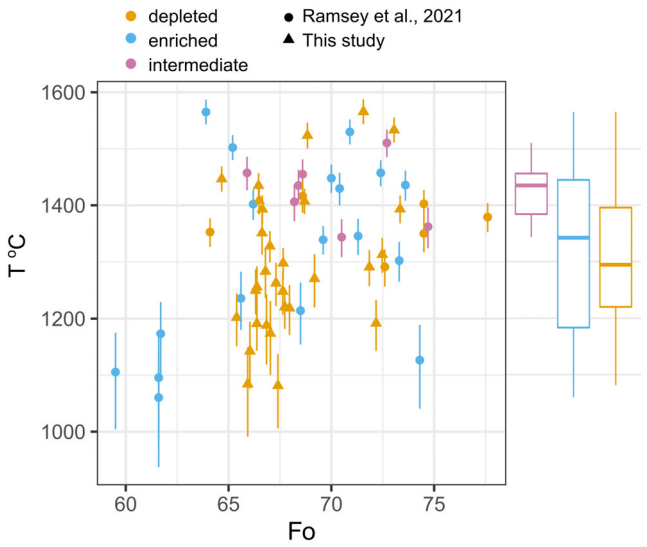

FIGURE 6. Al-in-olivine crystallization temperatures (°C) as a function of olivine forsterite content of SaU 005 (this study) and all measurements with <1000 ppm Al in olivine from Ramsey et al. (2021), excluding one of their olivine measurements of LAR 12095 with Al below the detection limit. Figures are color coded according to whether those samples are enriched, depleted (including Tissint) or intermediate. Uncertainties are all 2σ based on either counting statistics from Al measurement in olivine (for consistency with the present study, temperature uncertainties for the Ramsey et al. (2021) data are recalculated based on $\sigma_{Al_2O_3}$ of their repeat analyses of San Carlos olivine) or on the thermometer inherent uncertainty of 11°C, whichever is higher. Box plots of the temperature distribution are shown on the right-hand side.

The presence of "recent" (shergottite-aged) mantle plumes is consistent with the prediction of present-day mantle convection style by geodynamic models (Plesa et al., 2018).

The ΔT from thermometry is significantly less than the ΔT ~350–400°C temperature offset proposed for shergottites by Filiberto (2017) from a major element methodology: this proposed temperature elevation is very large compared to Earth mantle plumes and is not supported by thermometry evidence. Filiberto (2017) use a methodology whereby whole-rock compositions, corrected to primary magmas in equilibrium with Fo_{86} olivine, are used as the basis for Mg exchange thermometry and silica activity barometry. The inherent assumptions involved in correcting whole-rock compositions to primary ones are avoided here by just using a mineral thermometry method. In addition, slow-diffusing trace elements should be more robust than fast-diffusing Fe-Mg during high-temperature processing events such as impact melting.

CONCLUSIONS

Several geothermobarometry techniques for mafic and ultramafic systems that were developed for terrestrial

samples (e.g., Coogan et al., 2014; Köhler & Brey, 1990; Putirka, 2008) have be applied to extraterrestrial samples (Prissel et al., 2017a; Ramsey et al., 2021). Caution is needed when applying these techniques to meteorites, because of the additional complications caused by their more complex histories.

Olivine phenocrysts in olivine-phyric shergottites have the potential to record information about their formation conditions in their trace element contents. The solubility of Al in olivine is temperature dependent, forming the basis of the Al-in-olivine thermometer that would seem to be an ideal tool for determining near-liquidus crystallization temperatures, regardless of cooling history or knowledge of equilibrium melt composition. However, the shock and weathering history of meteorites may result in the local redistribution of trace elements within olivine crystals. Elements are not only redistributed by internal melting, the presence of melt veins also provides diffusive pathways for fluid-mobile elements to subsequently enter.

This study highlights that two olivine-phyric shergottites, both having experienced shock and terrestrial weathering, have different internal microstructures resulting from different post-formation pressure–temperature histories. Olivine phenocrysts in DaG 476 contain fine-scale and pervasive veining that is not easy to see in BSE imaging or by petrographic microscope. Veins, characterized by elevated K and Al concentrations, originate from within the crystals and extend to the sub-micron scale. They may originate from weathering alteration of shock melt. Accordingly, Al-in-olivine thermometry failed in this sample because Al concentrations were elevated and erratic. SaU 005 also shows microtextural evidence of shock alteration, including parallel deformation bands, conjugate fractures and exsolved grains. The alteration is of a different nature to DaG 476, perhaps because peak temperatures of alteration were lower, cooling was faster, and the terrestrial weathering history was shorter. It appears not to have resulted in the redistribution of elements beyond the formation of sparse exsolved intergrowths of clinopyroxene and spinel. It is possible to measure original Al concentrations by EPMA in this sample.

The average Al-in-olivine crystallization temperature in SaU 005 is 1300 ± 130°C, with a higher average of 1380 ± 150°C for the most primitive (Fo > 71) olivines. This is similar to published Al-in-olivine temperatures from a variety of other olivine-phyric shergottites (Ramsey et al., 2021). Combining the present data with the published data of Ramsey et al. (2021), it can be seen that there is no difference between crystallization temperatures in depleted, intermediate, and enriched shergottites. The average temperatures across all shergottites in Fo > 70 olivines is 1380°C. When adjusted for equilibrium with mantle olivine, this is around 1500°C. This temperature is high compared to estimates of the ambient Martian mantle, indicating a moderately hot mantle plume source for the olivine-phyric shergottites. Previous MELTS modeling and O isotope thermometry support this interpretation.

Acknowledgments—We gratefully acknowledge the loan of shergottite thin sections SaU 005 (P10386 off BM.2000, M40) and DaG 476 (P10078 off BM.2000,M7) by the National History Museum, London (MIN-2019-163-MET) and the assistance of Natasha Almeida. We are grateful to Kelsey Prissel and Geoffrey Howarth for insightful and thorough reviews and to Akira Yamaguchi for comments and editorial handling, all of which helped us to improve the manuscript considerably. We also thank James Darling for useful discussion.

Data Availability Statement—The data that support the findings of this study are available in the supplementary material of this article.

Editorial Handling—Dr. Akira Yamaguchi

REFERENCES

Baratoux, D., Toplis, M. J., Monnereau, M., and Gasnault, O. 2011. Thermal History of Mars Inferred from Orbital Geochemistry of Volcanic Provinces. *Nature* 472: 338–341.

Barrat, J. A., Blichert-Toft, J., Nesbitt, R. W., and Keller, F. 2001. Bulk Chemistry of Saharan Shergottite Dar al Gani 476. *Meteoritics & Planetary Science* 36: 23–30.

Boctor, N., Alexander, C. M. O'D., Wang, J., and Hauri, E. 2001. Shock Metamorphic Effects and Hydrogen Isotope Study of the Martian Meteorite Sayh al Uhaymir 005. *Meteoritics & Planetary Science* 36: A23.

Borg, L. E., Nyquist, L. E., Wiesmann, H., Shih, C.-Y., and Reese, Y. 2003. The Age of Dar al Gani 476 and the Differentiation History of the Martian Meteorites Inferred from their Radiogenic Isotopic Systematics. *Geochimica et Cosmochimica Acta* 67: 3519–36.

Chakraborty, S. 1997. Rates and Mechanisms of Fe-Mg Interdiffusion in Olivine at 980°–1300°C. *Journal of Geophysical Research: Solid Earth* 102: 12317–31.

Coogan, L. A., Saunders, A. D., and Wilson, R. N. 2014. Aluminum-in-Olivine Thermometry of Primitive Basalts: Evidence of an Anomalously Hot Mantle Source for Large Igneous Provinces. *Chemical Geology* 368: 1–10.

Danyushevsky, L. V., and Plechov, P. 2011. Petrolog3: Integrated Software for Modeling Crystallization Processes. *Geochemistry, Geophysics, Geosystems* 12: Q07021.

Dreibus, G., Spettel, B., Haubold, R., Jochum, K. P., Palme, H., Wolf, D., and Zipfel, J. 2000. Chemistry of a New Shergottite: Sayh al Uhaymir 005. *Meteoritics & Planetary Science Supplement* 35: A49.

Droop, G. T. R. 1987. A General Equation for Estimating Fe^{3+} Concentrations in Ferromagnesian Silicates and Oxides from Microprobe Analyses, Using Stoichiometric Criteria. *Mineralogical Magazine* 51: 431–35.

Filiberto, J. 2017. Geochemistry of Martian Basalts with Constraints on Magma Genesis. *Chemical Geology* 466: 1–14.

Goodrich, C. A. 2003. Petrogenesis of Olivine-Phyric Shergottites Sayh al Uhaymir 005 and Elephant Moraine A79001 Lithology A. *Geochimica et Cosmochimica Acta* 67: 3735–72.

Greshake, A., Fritz, J., and Stöffler, D. 2004. Petrology and Shock Metamorphism of the Olivine-Phyric Shergottite Yamato 980459: Evidence for a Two-Stage Cooling and a Single-Stage Ejection History. *Geochimica et Cosmochimica Acta* 68: 2359–77.

Greshake, A., and Stöffler, D. 1999. Shock Metamorphic Features in the SNC Meteorite Dar Al Gani 476. 30th Lunar and Planetary Science Conference, abstract #1377. https://www.lpi.usra.edu/meetings/LPSC99/pdf/1377.pdf.

Greshake, A., and Stöffler, D. 2000. Shock Related Melting Phenomena in the SNC Meteorite Dar Al Gani 476. 31st Lunar and Planetary Science Conference, abstract #1043 https://www.lpi.usra.edu/meetings/lpsc2000/pdf/1043.pdf.

Gross, J., Treiman, A. H., Filiberto, J., and Herd, C. D. K. 2011. Primitive Olivine-Phyric Shergottite NWA 5789: Petrography, Mineral Chemistry, and Cooling History Imply a Magma Similar to Yamato-980459. *Meteoritics & Planetary Science* 46: 116–133.

Heinonen, J. S., Jennings, E. S., and Riley, T. R. 2015. Crystallisation Temperatures of the Most Mg-Rich Magmas of the Karoo LIP on the Basis of Al-in-Olivine Thermometry. *Chemical Geology* 411: 26–35.

Herzberg, C., Asimow, P. D., Arndt, N., Niu, Y., Lesher, C. M., Fitton, J. G., Cheadle, M. J., and Saunders, A. D. 2007. Temperatures in Ambient Mantle and Plumes: Constraints from Basalts, Picrites, and Komatiites. *Geochemistry, Geophysics, Geosystems* 8: Q02006.

Herzberg, C., and Gazel, E. 2009. Petrological Evidence for Secular Cooling in Mantle Plumes. *Nature* 458: 619–622.

Horvath, D. G., Moitra, P., Hamilton, C. W., Craddock, R. A., and Andrews-Hanna, J. C. 2021. Evidence for Geologically Recent Explosive Volcanism in Elysium Planitia, Mars. *Icarus* 365: 114499.

Jennings, E. S., Gibson, S. A., and Maclennan, J. 2019. Hot Primary Melts and Mantle Source for the Paraná-Etendeka Flood Basalt Province: New Constraints from Al-in-Olivine Thermometry. *Chemical Geology* 529: 119287.

Khisina, N. R., and Lorenz, C. A. 2015. Dehydrogenation as the Mechanism of Formation of the Oriented Spinel-Pyroxene Symplectites and Magnetite-Hematite Inclusions in Terrestrial and Extraterrestrial Olivines. *Petrology* 23: 176–188.

Khisina, N. R., Wirth, R., Abart, R., Rhede, D., and Heinrich, W. 2013. Oriented Chromite–Diopside Symplectic Inclusions in Olivine from Lunar Regolith Delivered by "Luna-24" Mission. *Geochimica et Cosmochimica Acta* 104: 84–98.

Köhler, T. P., and Brey, G. P. 1990. Calcium Exchange between Olivine and Clinopyroxene Calibrated as a Geothermobarometer for Natural Peridotites from 2 to 60 kb with Applications. *Geochimica et Cosmochimica Acta* 54: 2375–88.

Lapen, T. J., Righter, M., Andreasen, R., Irving, A. J., Satkoski, A. M., Beard, B. L., Nishiizumi, K., Jull, A. J. T., and Caffee, M. W. 2017. Two Billion Years of Magmatism Recorded from a Single Mars Meteorite Ejection Site. *Science Advances* 3: e1600922.

McKenzie, D., and Bickle, M. J. 1988. The Volume and Composition of Melt Generated by Extension of the Lithosphere. *Journal of Petrology* 29: 625–679.

Mikouchi, T., and Miyamoto, M. 1998. Pyroxene and Olivine Microstructures in Nakhlite Martian Meteorites: Implication for their Thermal History. 29th Lunar and Planetary Science Conference, abstract #1574.

Mikouchi, T., Miyamoto, M., and McKay, G. A. 2001. Mineralogy and Petrology of the Dar al Gani 476 Martian Meteorite: Implications for its Cooling History and Relationship to Other Shergottites. *Meteoritics & Planetary Science* 36: 531–548.

Mikouchi, T., Yamada, I., and Miyamoto, M. 2000. Symplectic Exsolution in Olivine from the Nakhla Martian Meteorite. *Meteoritics & Planetary Science* 35: 937–942.

Miyahara, M., Ohtani, E., Ozawa, S., Kimura, M., el Goresy, A., Sakai, T., Nagase, T., Hiraga, K., Hirao, N., and Ohishi, Y. 2011. Natural Dissociation of Olivine to (Mg,Fe) SiO_3 perovskite and magnesiowüstite in a Shocked Martian Meteorite. *Proceedings of the National Academy of Sciences of the United States of America* 108: 5999–6003.

Nishiizumi, K., Masarik, J., Welten, K. C., Caffee, M. W., Jull, A. J. T., and Klandrud, S. E. 1999. Exposure History of New Martian Meteorite Dar AL Gani 476. 30th Lunar and Planetary Science Conference, abstract #1966.

Nyquist, L. E., Bogard, D. D., Shih, C.-Y., Greshake, A., Stöffler, D., and Eugster, O. 2001. Ages and Geologic Histories of Martian Meteorites. *Space Science Reviews* 96: 105–164.

Papike, J. J., Karner, J. M., Shearer, C. K., and Burger, P. V. 2009. Silicate Mineralogy of Martian Meteorites. *Geochimica et Cosmochimica Acta* 73: 7443–85.

Pätsch, M., Altmaier, M., Herpers, U., Kosuch, H., Michel, R., and Schultz, L. 2000. Exposure Age of the New SNC Meteorite Sayh al Uhaymir 005. *Meteoritics & Planetary Science Supplement* 35: A124.

Plesa, A.-C., Padovan, S., Tosi, N., Breuer, D., Grott, M., Wieczorek, M. A., Spohn, T., Smrekar, S. E., and Banerdt, W. B. 2018. The Thermal State and Interior Structure of Mars. *Geophysical Research Letters* 45: 12,198–12,209.

Prissel, T. C., Gross, J., and Draper, D. S. 2017a. Application of Olivine-Spinel Equilibria to Extraterrestrial Igneous Systems. 48th Lunar and Planetary Science Conference, abstract #2436.

Prissel, T. C., Gross, J., and Draper, D. S. 2017b. Origin of Olivine-Phyric Shergottites. Annual Meeting of the Meteoritical Society 2017 (LPI Contribution no. 1987), 6338.

Putirka, K. D. 2008. Thermometers and Barometers for Volcanic Systems. *Reviews in Mineralogy and Geochemistry* 69: 61–120.

Ramsey, S. R., Howarth, G. H., Udry, A., and Gross, J. 2021. Nickel–Manganese Variability in Olivine and Al-in-Olivine Thermometry for Olivine-Phyric Shergottites. *Meteoritics & Planetary Science* 56: 1597–1618.

Sharp, T. G., and de Carli, P. S. 2006. Shock Effects in Meteorites. In *Meteorites and the Early Solar System II*, edited by D. S. Lauretta, and H. Y. McSween, Jr., 653–677. University of Arizona Press, Tucson, AZ.

Shih, C.-Y., Nyquist, L. E., and Reese, Y. 2007. Rb-Sr and Sm-Nd Isotopic Studies of Martian Depleted Shergottites SaU 094/005. 38th Lunar and Planetary Science Conference, abstract #1745.

Spandler, C., and O'Neill, H. S. C. 2010. Diffusion and Partition Coefficients of Minor and Trace Elements in San Carlos Olivine at 1,300°C with some Geochemical Implications. *Contributions to Mineralogy and Petrology* 159: 791–818.

Tait, K. T., and Day, J. M. D. 2018. Chondritic Late Accretion to Mars and the Nature of Shergottite Reservoirs. *Earth and Planetary Science Letters* 494: 99–108.

Takenouchi, A., Mikouchi, T., and Yamaguchi, A. 2018. Shock Veins and Brown Olivine in Martian Meteorites: Implications for their Shock Pressure–Temperature Histories. *Meteoritics & Planetary Science* 53: 2259–84.

Treiman, A. H., and Filiberto, J. 2015. Geochemical Diversity of Shergottite Basalts: Mixing and Fractionation, and their Relation to Mars Surface Basalts. *Meteoritics & Planetary Science* 50: 632–648.

Van de Moortèle, B., Reynard, B., McMillan, P. F., Wilson, M., Beck, P., Gillet, P., and Jahn, S. 2007. Shock-Induced Transformation of Olivine to a New Metastable (Mg, Fe)$_2$SiO$_4$ Polymorph in Martian Meteorites. *Earth and Planetary Science Letters* 261: 469–475.

Van de Moortèle, B., Reynard, B., Rochette, P., Jackson, M., Beck, P., Gillet, P., McMillan, P. F., and McCammon, C. A. 2007. Shock-Induced Metallic Iron Nanoparticles in Olivine-Rich Martian Meteorites. *Earth and Planetary Science Letters* 262: 37–49.

Wadhwa, M., Lentz, R. C. F., McSween, H. Y., and Crozaz, G. 2001. A Petrologic and Trace Element Study of Dar al Gani 476 and Dar al Gani 489: Twin Meteorites with Affinities to Basaltic and Lherzolitic Shergottites. *Meteoritics & Planetary Science* 36: 195–208.

Walton, E. L., Sharp, T. G., Hu, J., and Filiberto, J. 2014. Heterogeneous Mineral Assemblages in Martian Meteorite Tissint as a Result of a Recent Small Impact Event on Mars. *Geochimica et Cosmochimica Acta* 140: 334–348.

Wan, Z., Coogan, L. A., and Canil, D. 2008. Experimental Calibration of Aluminum Partitioning between Olivine and Spinel as a Geothermometer. *American Mineralogist* 93: 1142–47.

Xu, R., and Liu, Y. 2016. Al-in-Olivine Thermometry Evidence for the Mantle Plume Origin of the Emeishan Large Igneous Province. *Lithos* 266–267: 362–66.

Yoshizaki, T., and McDonough, W. F. 2020. The Composition of Mars. *Geochimica et Cosmochimica Acta* 273: 137–162.

Zipfel, J. 2000. Sayh al Uhaymir 005/008 and its Relationship to Dar al Gani 476/489. *Meteoritics & Planetary Science Supplement* 35: A178–A106.

Zipfel, J., Scherer, P., Spettel, B., Dreibus, G., and Schultz, L. 2000. Petrology and Chemistry of the New Shergottite Dar al Gani 476. *Meteoritics & Planetary Science* 35: 95–106.

SUPPORTING INFORMATION

Additional supporting information may be found in the online version of this article.

Figure S1. Scans of the thin sections (a) DaG 476 (BM.2000,M7) and (b) SaU 005 (BM.2000,M40). Strong orange staining is apparent in the large central olivine macrocrysts in (a), with weaker staining in some other crystals and weak staining in (b). Horizontal FOV = approx. 1 cm for each image.

Figure S2. Compositions of SaU 005 olivine point analyses used in the thermometry in terms of Al_2O_3, Cr_2O_3, CaO, and NiO concentrations (wt%) and Fo content ($=100X_{Mg}/(X_{Mg} + X_{Fe})$).

Figure S3. Compositions of SaU 005 spinel inclusions used in the thermometry: Ti (per formula unit) as a function of Cr# ($=X_{Cr}/(X_{Cr}+X_{Al})$).

Table S1. Electron probe microanalysis data.

Table S2. Uncertainties on EPMA data presented in Table S1.